and 15° was observed among the four structures (Table 2). In the majority of these cases, the change in the χ_2 angle relative to the original design remained near the value of 25° observed in the initial BIF_1 structure. This result suggested that mutations to Ala^{79} and Trp^{123} have the desired effect of rotating ring B without affecting the absolute orientation of ring A. Unfortunately, substitution of Tyr^{123} with the beta-branched Val and the opposing Ala^{79} with Ser (BIF_1.1) had the effect of rotating ring B even farther out of plane (35°) than in the original structure (Fig. 3A). This undesired rotation was partially remedied in BIF_1.2 (Φ = 21°) (Fig. 3B) by substituting Ala^{79} with a bulkier Val residue and further corrected in BIF_1.3 and BIF_1.4 (Φ = 15° and 20°, respectively) (Fig. 3, C and D) by replacing the opposing Tyr^{123} with a smaller Ala residue and Ala^{79} with Ser (BIF_1.3) or Val (BIF_1.4). This analysis suggested that ring A could potentially be rotated into a coplanar geometry by further increasing the size of the amino acid at position 79 with an Ala^{79}Ile mutation while maintaining Phe^{42} and the Tyr^{123}Ala mutation. The additional methyl group of the isoleucine should force the side of ring A to rotate further in the desired direction.

We next generated the corresponding BIF_0 mutant (S^8A, I^{11}BiPhe, Y^{79}I, F^{81}W, K^{121}I, and F^{123}A), purified the protein, and solved its crystal structure to 2.05 Å resolution (Fig. 4). Analysis of the electron density showed that the two phenyl rings of BiPhe are coplanar, which matches the configuration of the TS for the bond rotation reaction. The structure of BIF_0 shows that, in addition to adding steric bulk beneath ring A, the V^{79}I mutation also forces the side chain of Phe^{77} to adopt a different rotamer than was observed in BIF_1.4, which has the effect of further rotating ring A into the plane of ring B (Fig. 4). The mutations introduced into BIF_0 do not appear to substantially affect the thermal stability of the protein. The melting temperature of this mutant, as determined by differential scanning calorimetry, was ~110°C, consistent with the 3D structure of BIF_0, which shows that the protein core is well packed.

We have shown by iterative computational design, mutagenesis, and protein structure determination that one can design a protein core that stabilizes a simple conformational transition state to such a degree that one can determine its 3D x-ray crystal structure. However, we should note that the biphenyl energy landscape corresponds to a substructure within the protein relative to the energetics of the global protein conformational ensemble. A similar strategy was recently employed to directly observe catalyst-substrate interactions through x-ray crystallographic analysis (*33*). The results described here may not be all that surprising given that enzymes typically stabilize a rate-limiting TS by 8 to 12 kcal/mol. Nonetheless, these experiments underscore the ability of proteins to fold into defined 3D structures in which van der Waals, hydrogen-bonding, and electrostatic interactions can be controlled with exquisite precision.

REFERENCES AND NOTES

1. T. S. Rose, M. J. Rosker, A. H. Zewail, *J. Chem. Phys.* **88**, 6672–6673 (1988).
2. J. C. Polanyi, A. H. Zewail, *Acc. Chem. Res.* **28**, 119–132 (1995).
3. R. Srinivasan, J. S. Feenstra, S. T. Park, S. Xu, A. H. Zewail, *Science* **307**, 558–563 (2005).
4. H. Ihee *et al.*, *Science* **291**, 458–462 (2001).
5. L. Pauling, *Chem. Eng. News* **24**, 1375–1377 (1946).
6. W. P. Jencks, *Catalysis in Chemistry and Enzymology* (Dover, Mineola, NY, 1987).
7. A. Tramontano, K. D. Janda, R. A. Lerner, *Science* **234**, 1566–1570 (1986).
8. S. J. Pollack, J. W. Jacobs, P. G. Schultz, *Science* **234**, 1570–1573 (1986).
9. P. G. Schultz, R. A. Lerner, *Science* **269**, 1835–1842 (1995).
10. S. Dwivedi, S. P. Kruparani, R. Sankaranarayanan, *Nat. Struct. Mol. Biol.* **12**, 556–557 (2005).
11. F. Ceccacci, G. Mancini, P. Mencarelli, C. Villani, *Tetrahedron Asymmetry* **14**, 3117–3122 (2003).
12. A. Almenningen *et al.*, *J. Mol. Struct.* **128**, 59–76 (1985).
13. J. E. Katon, E. R. Lippincott, *Spectrochimica Acta* **15**, 627–650 (1959).
14. L. A. Carreira, T. G. Towns, *J. Mol. Struct.* **41**, 1–9 (1977).
15. H. Suzuki, *Bull. Chem. Soc. Jpn.* **32**, 1340–1350 (1959).
16. O. Bastiansen, S. Samdal, *J. Mol. Struct.* **128**, 115–125 (1985).
17. J. Xie, W. Liu, P. G. Schultz, *Angew. Chem. Int. Ed.* **46**, 9239–9242 (2007).
18. L. Wang, A. Brock, B. Herberich, P. G. Schultz, *Science* **292**, 498–500 (2001).
19. J. K. Eloranta, *Zeitschrift Naturforschung Teil A* **27a**, 1652–1662 (1972).
20. Materials and methods are available as supplementary materials on *Science* Online.
21. A. Razvi, J. M. Scholtz, *Protein Sci.* **15**, 1569–1578 (2006).
22. J. D. Bloom, S. T. Labthavikul, C. R. Otey, F. H. Arnold, *Proc. Natl. Acad. Sci. U.S.A.* **103**, 5869–5874 (2006).
23. A. Zanghellini *et al.*, *Protein Sci.* **15**, 2785–2794 (2006).
24. G. B. McGaughey, M. Gagné, A. K. Rappé, *J. Biol. Chem.* **273**, 15458–15463 (1998).
25. S. M. Le Grand, K. M. Merz, *J. Comput. Chem.* **14**, 349–352 (1993).
26. B. Kuhlman, D. Baker, *Proc. Natl. Acad. Sci. U.S.A.* **97**, 10383–10388 (2000).
27. M. C. Lawrence, P. M. Colman, *J. Mol. Biol.* **234**, 946–950 (1993).
28. A. Chatterjee, M. J. Lajoie, H. Xiao, G. M. Church, P. G. Schultz, *ChemBioChem* **15**, 1782–1786 (2014).
29. L. J. Shimon *et al.*, *Structure* **5**, 381–390 (1997).
30. S. Dwivedi, S. P. Kruparani, R. Sankaranarayanan, *Acta Crystallogr. D Biol. Crystallogr.* **60**, 1662–1664 (2004).
31. Y. Tanaka *et al.*, *Proteins* **61**, 1127–1131 (2005).
32. M. S. Cosgrove *et al.*, *Biochemistry* **45**, 7511–7521 (2006).
33. S. Han, B. V. Le, H. S. Hajare, R. H. G. Baxter, S. J. Miller, *J. Org. Chem.* **79**, 8550–8556 (2014).

ACKNOWLEDGMENTS

The authors thank N. P. King and P.-S. Huang for helpful discussions. D.B and J.H.M. were supported by the Defense Threat Reduction Agency (HDTRA1-11-1-0041). J.H.M. was supported by National Institute of General Medical Science of the National Institutes of Health under award F32GM099210. P.G.S. acknowledges support by the National Institutes of Health under award 2 R01 GM097206-05. The content is solely the responsibility of the authors and does not represent the official views of the National Institutes of Health. Structures of BIF_1, BIF_1.1 to BIF_1.4, and BIF_0 have been deposited in the Protein Data Bank under accession numbers 4S02, 4S0J, 4S0L, 4S0I, 4S0K, and 4S03.

SUPPLEMENTARY MATERIALS

www.sciencemag.org/content/347/6224/863/suppl/DC1
Materials and Methods
Figs. S1 and S2
Tables S1 and S2
References (*34*–*42*)

6 November 2014; accepted 20 January 2015
10.1126/science.aaa2424

ANIMAL EVOLUTION

Cope's rule in the evolution of marine animals

Noel A. Heim,[1]* Matthew L. Knope,[1]† Ellen K. Schaal,[1]‡ Steve C. Wang,[2] Jonathan L. Payne[1]

Cope's rule proposes that animal lineages evolve toward larger body size over time. To test this hypothesis across all marine animals, we compiled a data set of body sizes for 17,208 genera of marine animals spanning the past 542 million years. Mean biovolume across genera has increased by a factor of 150 since the Cambrian, whereas minimum biovolume has decreased by less than a factor of 10, and maximum biovolume has increased by more than a factor of 100,000. Neutral drift from a small initial value cannot explain this pattern. Instead, most of the size increase reflects differential diversification across classes, indicating that the pattern does not reflect a simple scaling-up of widespread and persistent selection for larger size within populations.

Body size constrains key ecological and physiological traits such as generation time, fecundity, metabolic rate, population size, and home range size (*1*, *2*). Because of perceived advantages associated with larger size, there has long been speculation that animals tend to increase in size over evolutionary time (*3*–*8*), a pattern commonly referred to as Cope's rule. Fossil data support size increase in many cases (*6*, *9*–*15*), but numerous counterexamples also exist (*16*–*22*). Moreover, some instances of size increase could simply result from neutral drift away from an initially small size rather than requiring any active selection for size (*17*, *22*).

To determine whether animal sizes have increased since the start of the Cambrian [542 million

[1]Department of Geological and Environmental Sciences, Stanford University, 450 Serra Mall, Stanford, CA 94305, USA. [2]Department of Mathematics and Statistics, Swarthmore College, Swarthmore, PA 19081, USA.
*Corresponding author. E-mail: naheim@stanford.edu †Present address: Department of Biology, Stanford University, Stanford, CA 94305, USA. ‡Present address: Department of Geology, Lawrence University, Appleton, WI 54911, USA.

years ago (Ma)] and, if so, whether the increase can be accounted for by neutral drift or requires active evolutionary processes, we compiled adult body size measurements for 17,208 genera of marine animals from the phyla Arthropoda, Brachiopoda, Chordata, Echinodermata, and Mollusca, with stratigraphic ranges in the fossil record resolved to stages, the finest temporal units in the global geologic time scale (*23*) (fig. S1A). These phyla together account for 74% of animal diversity in the fossil record (*24*), and our data set covers 75% of total known genus diversity in these phyla. We measured the three major body axes from published images of specimens (typically holotypes of the type species) (*23*) in order to estimate the size of each genus as a simple geometric solid or from known length:mass relationships (*23*). We used linear regressions of biovolume on maximum length for classes and phyla to estimate the biovolume of genera for which fewer than three major axes were illustrated (*23*) (fig. S2 and table S1).

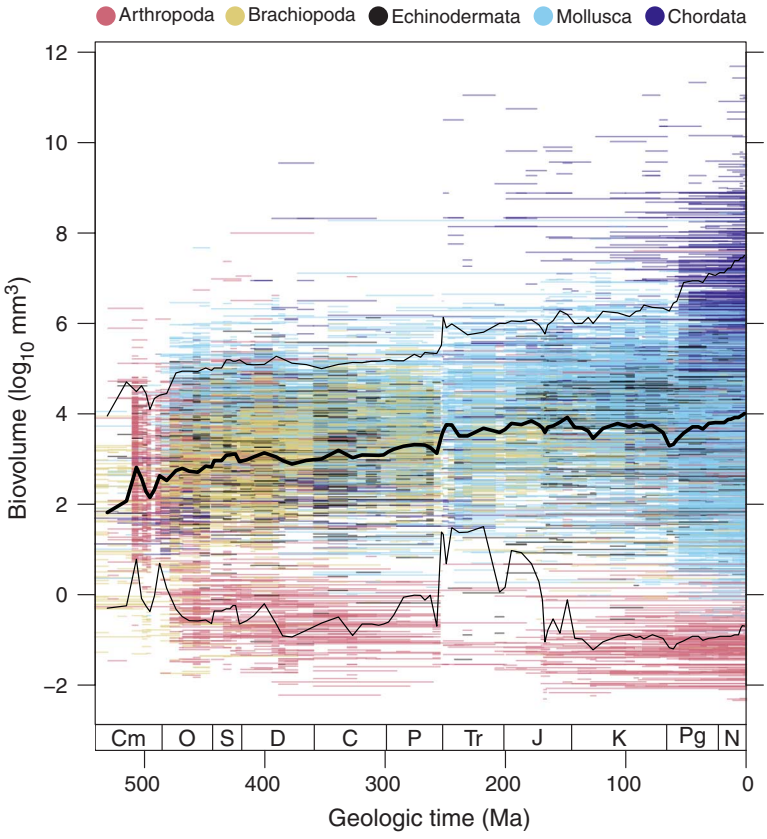

Fig. 1. Body size evolution across the past 542 million years. The distribution of fossil marine animal biovolumes across the Phanerozoic is shown. The colored horizontal lines show genus durations. The thick black line indicates the stage-level mean body size. The thin black lines demarcate the 5th and 95th percentiles. Cm, Cambrian; O, Ordovician; S, Silurian; D, Devonian; C, Carboniferous; P, Permian; Tr, Triassic; J, Jurassic; K, Cretaceous; Pg, Paleogene; N, Neogene.

Figure 1 illustrates the sizes of the marine animal genera in our data set across the past 542 million years. The mean biovolume across genera has increased by more than a factor of 150 (2.18 $\log_{10}$ units; the median increased by 2.35 $\log_{10}$ units) since the earliest Cambrian. Over the same interval, the range in biovolume expanded from 8 orders of magnitude in the Cambrian to 14 orders of magnitude in the Pleistocene (1 Ma). Most of this expansion in size range reflects an increase in the maximum, which climbed by more than three orders of magnitude between the Early Cambrian and Middle Devonian (542 to 385 Ma) and by an additional two orders of magnitude thereafter. In contrast, the overall minimum size decreased by less than one order of magnitude between the Early Cambrian and Middle Devonian and has remained stable ever since.

To test models of neutral change relative to active processes, we compared observed trends in maximum, mean, and minimum size to expectations generated by three evolutionary branching models: an unbiased random walk (i.e., Brownian motion; fig. S3A), a bounded random walk (i.e., Brownian motion with a reflecting lower bound; fig. S3B), and a size-biased random walk (fig. S3C) (*23*). The size-biased model fit observed trends in the minimum, mean, and maximum size better than the neutral and lower-bounded models (Fig. 2 and fig. S4). The observed minimum size is within the predicted range of all three models,

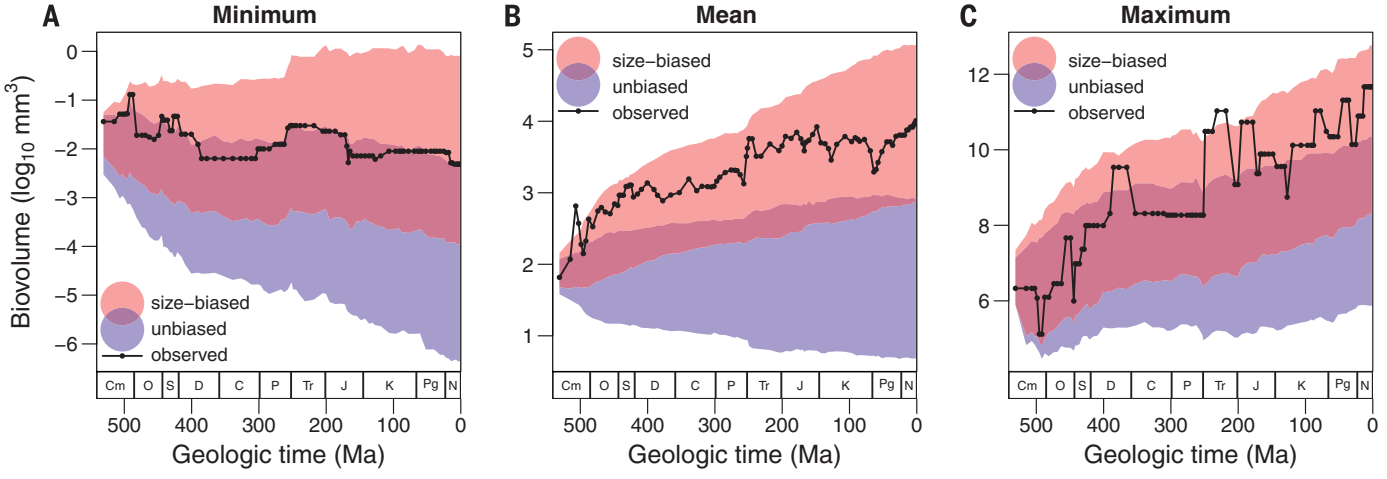

Fig. 2. Comparison of observed biovolume trends to those obtained from stochastic branching models (***23***). The colored regions highlight the size space occupied by 90% of the 1000 model runs. For clarity, only results for the size-biased (red) and unbiased (blue) models are shown; except below the minimum size, the lower-bounded model produced results nearly identical to the unbiased model (fig. S4). (**A**) Minimum, (**B**) mean, and (**C**) maximum sizes. Time scale abbreviations are the same as in Fig. 1.

but the observed mean and maximum sizes trended above the predicted range for the unbiased and lower-bounded models (Fig. 2 and fig. S4). As an additional test of the three models, we compared the observed distribution of biovolumes of all 2280 Pleistocene genera, the most recent and taxonomically diverse time interval in our analyses, to distributions predicted by our branching models and found strong support for the size-biased model over the other two models (table S2) (*23*). Finally, we used an independent, likelihood-based approach to compare support among five models for the trend in mean size over the entire 542 million years (*23*). Three models assumed a single mode of size evolution across the Phanerozoic (driven trend, random walk, or stasis). The best-supported of these models was the driven trend toward larger size (Table 1). However, allowing a shift in model type and parameters at the era-bounding mass extinctions improved the overall model fit, with the best-fit model in the Paleozoic being a driven trend toward larger size, followed by stasis in the Mesozoic, and a reversion to a driven trend in the Cenozoic (*23*) (Table 1). Removing the marine tetrapods, which tend to be very large, did not change this result (table S3). Thus, most of Phanerozoic time has been characterized by a trend toward larger animal sizes.

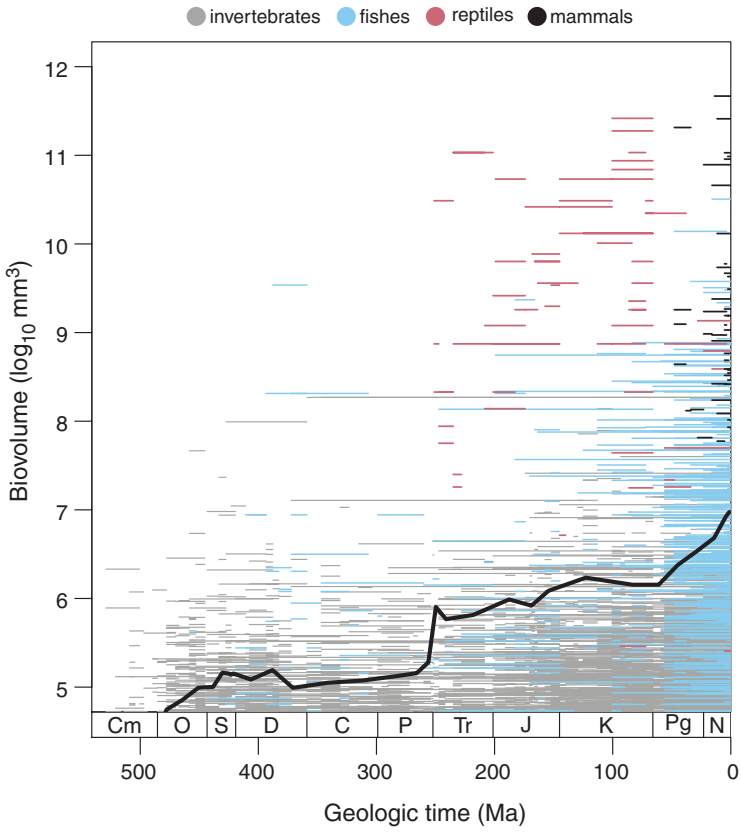

Fig. 3. Taxonomic compositions of the largest genera. Fishes and, later, air-breathing tetrapods, dominate the top of the size distribution. All genera with epoch- or stage-resolved stratigraphic ranges are plotted here, allowing for the inclusion of more large vertebrates. Horizontal lines show genus durations. The heavy black line demarcates the 95th percentile of all genera. Time scale abbreviations are the same as in Fig. 1.

The trends in minimum, mean, and maximum biovolume of marine animals are consistent with actively driven size increase and not consistent with simple neutral drift away from an initially small ancestor. To determine the extent to which this trend reflects size increase at low taxonomic levels across all phyla versus differential diversification of higher taxa with different mean sizes, we compared the observed trend in the mean to the expected trend if size were kept constant as diversity changed within different levels of the Linnaean hierarchy (fig. S5). This comparison demonstrates that much of the observed size increase reflects differential diversification among classes and is consistent with hierarchical size evolution in Paleozoic brachiopods (*15*). This finding also sheds light on the tripartite nature of the Phanerozoic trend in mean biovolume, as there was little differential diversification among classes during Mesozoic time (fig. S1B).

The dominance of differential diversification at the class level in producing the overall trend toward larger animal sizes emphasizes the hierarchical nature of evolutionary processes. In addition, it suggests that the widespread bias toward selection for larger size observed in extant populations (*8*) is unlikely to propagate into large-scale evolutionary trends observed in the fossil record. If the Phanerozoic trend reflected widespread selection for larger size at low taxonomic levels, we would expect to see most of the size trend explained by size increase within families, the lowest taxonomic level at which we can aggregate our data. These findings suggest that the factors favoring the overall trend toward larger size in marine animals relate to basic body plan and ecological life mode rather than competitive advantages associated with size differences within populations. These findings do not rule out an additional, smaller component related to widespread selection for larger size within populations, as there is also a component of size increase that occurs within families (fig. S5).

The taxonomic composition of the smallest and largest genera over time suggests the operation

Table 1. Results of model comparisons for the Phanerozoic trend in mean biovolume. Lower corrected Akaike information criterion (AICc) and higher Akaike weights indicate more support for a given model. logL is the log likelihood, and *K* is the number of free parameters in each model. The two-phase model has a break point at the Permian/Triassic boundary. The three-phase model has break points at the Permian/Triassic and Cretaceous/Paleogene boundaries. The best-fit model for each phase is used in multiphase models. The three-phase model is the best-supported model. See the supporting materials for details of the statistical methods (*23*). n/a, not applicable.

	logL	AICc	*K*	Akaike weight	Akaike weight single-phase model comparison
Random walk	53.7	-103.3	2	0.000	0.305
Driven trend	55.6	-104.9	3	0.000	0.695
Stasis	-63.7	131.5	2	0.000	0.000
Two-phase (driven trend/random walk)	60.5	-110.4	5	0.001	n/a
Three-phase (driven trend/stasis/driven trend)	71.2	-124.8	8	0.999	n/a

of constraints at the size extremes, even if these constraints are not required to model the overall distribution of animal sizes. The size minimum has been populated nearly exclusively by ostracods (a class of exclusively small-bodied crustaceans) since Silurian time (420 Ma). With the exception of the Middle/Late Triassic (235 Ma), where there is a maximum in ostracod size and a minimum in other animals, no other group in our data set comes within a factor of 6 of the smallest ostracod. The size maximum has been populated entirely by chordates since the Early Triassic (252 Ma), with no other genus since then coming within a factor of 2.5 of the largest chordate.

The dominance of a single phylum at each end of the size spectrum could result from simple incumbency effects, but transitions over time in the class affinities of the largest marine chordates suggest that physiology is also an important constraint, at least on the overall maximum size of marine animals. Nearly all of the largest solitary marine bilaterian genera have been reptiles and mammals. Tetrapods first reinvaded the oceans during Late Permian time (260 Ma) and rapidly occupied the size maximum (Fig. 3). Reptiles continued to dominate the top end of the size spectrum during the Mesozoic. Cetaceans were the first mammals to evolve a marine lifestyle and have occupied the largest marine body sizes since they first invaded the oceans during the Eocene (48 Ma) (Fig. 3). Air breathing is an exaptation (*25*) that can explain the rapid and widespread attainment of large size in marine reptiles and mammals. Relative to water, air has 20 to 30 times the concentration of O_2, is up to 100 times less viscous, has diffusion rates of O_2 through membranes that are 300,000 times faster, and is about 1000 times less dense (*26*). Thus, large animals are better able to meet their metabolic needs by breathing air than by breathing water. In fact, O_2 limitation has been proposed as a mechanism for limiting the evolutionary emergence of large, free-swimming, predatory bilateria generally (*27*, *28*).

Synoptic size data show that the average size of marine animals has increased substantially since the Cambrian and that this increase reflects differential diversification of large-bodied classes rather than neutral drift. A remaining question is the extent to which this differential diversification was enabled by intrinsic factors such as physiology, escalatory interactions between predators and prey (*29*), or changes in the physical and non-animal environment, such as oxygen availability (*30*) or the amount and quality of primary production (*7*). Testing among these controls will be critical to understanding how the physical and biological environments combine to shape the evolution of global ecosystems.

REFERENCES AND NOTES

1. R. H. Peters, *The Ecological Implications of Body Size* (Cambridge Univ. Press, Cambridge, 1983).
2. J. H. Brown, *Macroecology* (Univ. of Chicago Press, Chicago, 1995).
3. E. D. Cope, *Am. Nat.* **19**, 234–247 (1885).
4. E. D. Cope, *The Primary Factors of Organic Evolution* (Open Court, London, 1896).
5. C. J. J. Depéret, *The Transformations of the Animal World* (Paul, Trench, Trübner; London, 1909).
6. N. D. Newell, *Evolution* **3**, 103–124 (1949).
7. R. K. Bambach, *Paleobiology* **19**, 372–397 (1993).
8. J. G. Kingsolver, D. W. Pfennig, *Evolution* **58**, 1608–1612 (2004).
9. B. Rensch, *Evolution* **2**, 218–230 (1948).
10. J. Alroy, *Science* **280**, 731–734 (1998).
11. A. J. Arnold, D. C. Kelly, W. C. Parker, *J. Paleontol.* **69**, 203–210 (1995).
12. B. A. Maurer, *Evol. Ecol.* **12**, 925–934 (1998).
13. M. Laurin, *Syst. Biol.* **53**, 594–622 (2004).
14. D. W. E. Hone, T. M. Keesey, D. Pisani, A. Purvis, *J. Evol. Biol.* **18**, 587–595 (2005).
15. P. M. Novack-Gottshall, M. A. Lanier, *Proc. Natl. Acad. Sci. U.S.A.* **105**, 5430–5434 (2008).
16. D. Jablonski, *Nature* **385**, 250–252 (1997).
17. S. J. Gould, *J. Paleontol.* **62**, 319–329 (1988).
18. D. S. Moen, *J. Evol. Biol.* **19**, 1210–1221 (2006).
19. M. J. Monroe, F. Bokma, *J. Evol. Biol.* **23**, 2017–2021 (2010).
20. R. J. Butler, A. Goswami, *J. Evol. Biol.* **21**, 1673–1682 (2008).
21. J. H. Knouft, L. M. Page, *Am. Nat.* **161**, 413–421 (2003).
22. S. M. Stanley, *Evolution* **27**, 1–26 (1973).
23. Materials and methods are available as supplementary materials on *Science* Online.
24. J. J. Sepkoski Jr., *Bull. Am. Paleontol.* **363**, 1–500 (2002).
25. S. J. Gould, E. S. Vrba, *Paleobiology* **8**, 4–15 (1982).
26. D. Pauly, *Gasping Fish and Panting Squids: Oxygen, Temperature and the Growth of Water-Breathing Animals* (International Ecology Institute, Oldendorf, Germany, 2010).
27. T. W. Dahl *et al.*, *Proc. Natl. Acad. Sci. U.S.A.* **107**, 17911–17915 (2010).
28. E. A. Sperling *et al.*, *Proc. Natl. Acad. Sci. U.S.A.* **110**, 13446–13451 (2013).
29. G. J. Vermeij, *Annu. Rev. Ecol. Syst.* **25**, 219–236 (1994).
30. H. D. Holland, *Philos. Trans. R. Soc. London Ser. B* **361**, 903–915 (2006).

ACKNOWLEDGMENTS

We thank G. Griggs, M. Faerber, M. Laws, S. Sanghvi, L. Taylor, and the many undergraduate and high-school students for making body size measurements. J. Saltzman helped recruit high-school students. G. Hunt assisted with time series analysis. A. Clauset and M. A. Etnier kindly made their body size data on extant marine mammals available. Funding was provided by NSF grant EAR-1151022, the Stanford School of Earth Sciences, and the Swarthmore College James Michener Faculty Fellowship. Raw data files used for all analyses are permanently archived in the Stanford Digital Repository (http://purl.stanford.edu/rf761bx8302). This is Paleobiology Database publication 217.

SUPPLEMENTARY MATERIALS

www.sciencemag.org/content/347/6224/867/suppl/DC1
Materials and Methods
Figs. S1 to S6
Tables S1 to S3
Caption for Database S1
References (*31*–*120*)

18 August 2014; accepted 19 December 2014
10.1126/science.1260065

SPATIAL NAVIGATION

Disruption of the head direction cell network impairs the parahippocampal grid cell signal

Shawn S. Winter,* Benjamin J. Clark,*† Jeffrey S. Taube‡

Navigation depends on multiple neural systems that encode the moment-to-moment changes in an animal's direction and location in space. These include head direction (HD) cells representing the orientation of the head and grid cells that fire at multiple locations, forming a repeating hexagonal grid pattern. Computational models hypothesize that generation of the grid cell signal relies upon HD information that ascends to the hippocampal network via the anterior thalamic nuclei (ATN). We inactivated or lesioned the ATN and subsequently recorded single units in the entorhinal cortex and parasubiculum. ATN manipulation significantly disrupted grid and HD cell characteristics while sparing theta rhythmicity in these regions. These results indicate that the HD signal via the ATN is necessary for the generation and function of grid cell activity.

The ability to navigate is critical for survival of all animals and relies on a broad network of hippocampal and limbic brain circuits (*1*, *2*). The parahippocampal cortex contains grid cells, which fire at multiple locations, forming a hexagonal pattern covering the entire environment (*3*, *4*). Computational models explain grid cell generation from combined inputs of distance and direction displacement, which can subsequently be used for path integration (*5*–*7*). Theta rhythm is thought to be necessary for the computation of distance in grid cell models, and disruption of this signal eliminates gridlike firing patterns (*8*, *9*). HD cells fire as a function of an animal's directional orientation in the horizontal plane and are thought to convey the directional heading component to grid cells. However, some models use movement-direction cells, which have yet to be experimentally verified (*10*). The HD cell signal is generated subcortically and then projected rostrally via the anterior thalamic nuclei (ATN) to the parahippocampal cortices (*2*, *11*, *12*). Two nuclei within the ATN are known to contain HD cells—the anterodorsal and anteroventral thalamic nuclei (*13*, *14*). We tested the role of the HD signal in generating grid cell activity in the parahippocampal cortices.

Experiment 1 recorded from parahippocampal cortex, including medial entorhinal cortex (MEC) and parasubiculum, while female Long-Evans rats

Department of Psychological and Brain Sciences, Center for Cognitive Neuroscience, Dartmouth College, Hanover, NH 03755, USA.
*These authors contributed equally to this work. †Present address: Department of Psychology, University of New Mexico, Albuquerque, NM 87131, USA. ‡Corresponding author. E-mail: jeffrey.taube@dartmouth.edu

www.sciencemag.org/content/347/6224/867/suppl/DC1

Supplementary Materials for

Cope's rule in the evolution of marine animals

Noel A. Heim,* Matthew L. Knope, Ellen K. Schaal, Steve C. Wang, Jonathan L. Payne

*Corresponding author. E-mail: naheim@stanford.edu

Published 20 February 2015, *Science* **347**, 867 (2015)
DOI: 10.1126/science.1260065

This PDF file includes:

Other Supplementary Materials for this manuscript includes the following:

Databases S1 stored in the Stanford Digital Repository: Raw tab-delimited data file. http://purl.stanford.edu/rf761bx8302

Materials and Methods

Taxonomic Data

Taxonomic assignments for the genera in our dataset were taken from the published sources containing stratigraphic ranges (*24*) or the measured illustrations, and then cross-referenced with the Paleobiology Database to check for synonymies and changes in rank. The taxonomic nomenclature in the Paleobiology Database represents the most current taxonomic opinions, where they exist in the database, so we have given precedence to those opinions. We used version 1.1 taxonomic services to retrieve taxonomic data from the Paleobiology Database (http://paleobiodb.org/data1.1/taxa). As is typical for synoptic studies of the fossil record (e.g., *31-33*), we treated subgenera as genera to avoid issues of taxonomic uncertainty below the genus level.

Only solitary, bilaterian marine animals were included in these analyses. These include genera from the phyla Arthropoda, Brachiopoda, Chordata, Echinodermata, and Mollusca. We excluded the phyla Bryozoa, Cnidaria, Hemichordata, and Porifera. These colonial and solitary non-bilaterian groups were excluded because size of a colonial animal is difficult to define and compare to solitary organisms and because controls on size evolution in sponges and diplobasts may differ fundamentally from those on triploblasts. Measuring an individual corallite or zooid is straightforward, but genetically identical corallites/zooids interconnect to form colonies. This presents a problem when comparing the sizes of solitary and colonial forms. Furthermore, most fossil colonies are represented in the fossil record as fragments, making measurement of colony size difficult to impossible. The four excluded phyla constitute less than 25% of known marine animal genera in the fossil record, and thus their exclusion is unlikely to change the overall trends in observed body size. Similarly, we have excluded the Cambrian fossils typically known as "small shelly fossils." These fossils are typically known only from isolated sclerites whose taxonomic affinities are unknown, even at the phylum level.

Biovolume Data

Body size measurements were made primarily from published figures of fossil specimens, typically the holotype of the type species. Although there is a slight tendency for figured specimens in monographs to be slightly larger than specimens from field-collected bulk samples, the bias is small, consistent across time and taxa, and has very little effect on analyses

of body size based on monographs (*34*). Furthermore, the size of the type species is an unbiased estimate of the median body size of species within a genus (*35*). Most of our measurements were made from the Treatise on Invertebrate Paleontology (*36-54*). Gastropod sizes were supplemented with measurements from the *Handbuch der Paläozoologie* [Handbook of Paleozoology] (*55*) and ostracod sizes were supplemented with the *Catalogue of Ostracoda* (56). Body sizes of extant bivalves from the *Compendium of Bivalves* (*57*) were also included. Vertebrates were measured from a variety of sources. Fish measurements were taken from *Fossil Atlas, Fishes* (*58*) and Fundamentals of Paleontology (*59*). Marine mammal sizes were taken from the primary literature (*60,61*). Marine reptiles were measured from *Handbuch der Paläoherpetologie* [Handbook of Paleoherpetology] (*62*) and *SeaLifeBase* (*63*). We also used a variety of published and database sources (*64-97*) for marine reptile genera. For extant vertebrate genera with a fossil record, we used size measurements from living representatives, which were made from the primary literature (*98,99*) and the online databases *SeaLifeBase* (*63*) and *FishBase* (*100*).

All sizes analyzed in this study are biovolumes in units of cubic millimeters. Most sizes were estimated from illustrated specimens, where we estimated biovolume as an ellipsoid based on the length of the three major body axes of the specimen. We estimated biovolume as a cone based on aperture diameter and total length of the shell for scaphopods, uncoiled cephalopods, heteromorphic ammonites, and rudist bivalves. In cases where fewer than three of the major axes were measurable from the figure, we estimated the biovolume from a linear regression of $\log_{10}$ biovolume on $\log_{10}$ maximum length based on specimens where we were able to measure all major axes (Fig. S2; Table S1). When possible, linear regressions for estimating biovolume from maximum length were performed at the class level, but in a very small number of cases where we could not assign a genus to a class (mostly Cambrian arthropods) we used a phylum-level linear regression (Fig. S2). This approach was used for the majority of genera lacking three axial measurements, but an alternative mass-based approach was necessary for the tetrapods and some extant fish.

Illustrations of whole tetrapods were typically unavailable; instead, authors often reported maximum body lengths. To create regression plots for mammals and reptiles, we used length to mass relationships for extant taxa to estimate mass, then converted mass to volume using known body densities. For fossil mammals, we used the total length to mass equation for extant marine

mammals reported by Silva (*101*), and for marine reptiles we used the extant terrestrial lizard snout-to-vent length to mass equation reported by Meiri (*102*). Additionally, body sizes for many of extant vertebrate genera were reported as masses. For these genera and for the genera for which we estimated mass from length, we converted mass to volume using tissue densities. We used a density of 1.03 g * cm^{-3} for mammals and reptiles (*103*), which is based on the estimated density of five sperm whale specimens; we are assuming extinct marine reptiles and mammals had a similar density as living cetaceans. We used a density of 1.06 g * cm^{-3} for fish (*104,105*) based on living sharks and teleost fishes. Although we have attempted to address small differences in overall density among these groups, any reasonable values for the tissue density of these marine animals will make no difference to our results because the difference between the density of seawater (1.026 g * cm^{-3}) and the maximum density used here is only 0.014 log-units.

In our analyses, we applied only one biovolume estimate for the entire stratigraphic range of a genus. This approach assumes that the size of the type specimen of a genus is representative for that genus throughout its duration. In instances where we have more than one biovolume measurement for a genus, we give priority to the size of the type specimen of the type species (typically from the Treatise on Invertebrate Paleontology (*36-54*)). In the absence of the holotype, we use the maximum size in order to reduce the possibility that we are including juveniles. The use of a single measurement per genus is reasonable given that size variation among genera is much greater than size variation within genera (*106,107*), and so this approach is valid at the scale of this study.

The selective nature of fossil preservation is always a concern when trying to draw broad conclusions from paleontological data. Despite the paucity of soft-bodied animals and other biases in the fossil record, our dataset accurately captures the full range of body sizes occupied by the phyla studied here. Size biases in the fossil record generally favor the preservation of large individuals (*108-110*), which will favor capturing the maximum size of skeletonized animals. Additionally, most of the largest taxa in the modern ocean tend to have mineralized hard parts that are easily fossilizable. Although there were large soft-bodied animals in the geologic past (e.g., Cambrian Medusozoa that were 50 cm in diameter (*111*)), there are no post-Cambrian lagerstätte with soft-bodied animals that approach size maxima for all marine animals. This observation suggests that the largest marine animals have been skeletonized for the vast majority of Phanerozoic time.

Stratigraphic Range Data

Stratigraphic ranges for genera were obtained from the *Treatise on Invertebrate Paleontology* (*36-54*), Sepkoski's *A Compendium of Fossil Marine Genera* (*24*), and the *Handbook of Paläeozology* (55; gastropods only). We only included genera in this study that have a body size measurement and a stage-resolved stratigraphic range, with the exception of the first four Cambrian stages. Because of small sample sizes and difficulties in correlating older stratigraphic nomenclature with current Early Cambrian stages, we used the first two Cambrian epochs (i.e., Terreneuvian and Series 2) rather than stages for the first 20 million years of the Cambrian. Consequently, we included genera with epoch-resolved stratigraphic ranges and first occurrences during the first two epochs of the Cambrian. In those instances where we have more than one stage-resolved stratigraphic range (or epoch-resolved as just described), we used the most recently published range. In most cases, this is the Sepkoski range; in a few cases we used the revised *Treatise on Invertebrate Paleontology* volumes for a more recently compiled stratigraphic range. Our estimates of genus richness for the Phanerozoic adequately capture total known diversity (Fig. S1A). The Pearson product-moment correlation between the number of genera in our dataset and the number of genera in Sepkoski (five studied phyla only) (*24*) is 0.99 on the raw time series and 0.86 on the first differences (both p-values $<< 0.001$).

Time Series Analysis of Mean

Statistical analysis of the trend in mean biovolume was performed using the *paleoTS* package for R (*112*). We used the "joint" parameterization of the models, which considers the joint distribution of all observed trait values rather than considering each pair of adjacent time intervals independently (i.e., first differences) and did not pool variances across samples (*113-114*). The analytical results in Table 1 compare five evolutionary models of trait evolution, biovolume in this case, and we use likelihood methods to determine which model best describes the observed data (*113-114*). The five models compared are a random walk, driven trend (i.e., generalized random walk), stasis, two-phase model with a break point at the Permian/Triassic boundary, and three-phase model with breakpoints at the Permian/Triassic and Cretaceous/Paleogene boundaries (*113-115*). In the random walk model, the change in trait mean is equal to the mean in the previous interval plus some change drawn from a normal distribution

with a mean of zero. The driven trend model is similar to the random walk model, except the size change is drawn from a normal distribution with a nonzero mean. For the two- and three-phase models, each segment was evaluated for the best-fit model: unbiased random walk, driven trend, or stasis. The Paleozoic and Cenozoic segments are each best fit by a driven trend while the Mesozoic is best fit by stasis, and the post-Paleozoic segment is best fit by an unbiased random walk. The total number of free parameters in the segmented models is equal to the sum of the free parameters in each segment. Since we choose the breakpoints rather than determining them algorithmically, they were not treated as free parameters. Note that choosing breakpoints based upon visual inspection of the mean trend rather than objectively finding the best breakpoints has the potential to unduly favor the Driven Trend/Stasis/Driven Trend model as our statistical hypothesis is not developed independently of the data. Excluding the secondarily aquatic marine reptiles and mammals does not change the best-fit model for each segment or reduce the statistical support for a three-phase model of the mean (Table S3).

Branching Models

To evaluate the likelihood that the minimum, mean, and maximum biovolumes in our data are consistent with biased or unbiased size evolution, we ran simulations of each model presented in Figure 1 following the same branching process (*116*) and constrained by observed Phanerozoic rates of origination and extinction. Each model run proceeded through 541 one-million-year time increments. The first time interval of each run was seeded with 99 genera, the number present in the first Cambrian epoch (Terreneuvian). Each initial taxon was assigned its observed Terreneuvian biovolume. Origination and extinction probabilities for each time step varied through time and were based on the percent extinction and origination rates observed in this dataset. Although per capita rates are preferred in most macroevolutionary studies (*117*), percent rates have the advantage of ranging between 0 and 1. This property allows us to treat the rates as probabilities in our model; per capita rates vary between 0 and ∞ thus cannot be treated as a probability, as needed in our model. We calculated a continuous percent per million-year rate for each stage and then performed a loess nonparametric regression with a span of 10% on the full time series in order to calculate rates for each one-million-year time increment. The use of a relatively small span in the regression preserves the observed temporal volatility in the observed per-stage rates (i.e., ensuring that we are not over-smoothing).

During each time step, extant taxa were randomly selected for extinction based on the extinction rate for that interval. After extinction, a randomly selected subset of the survivors was selected to produce daughter taxa, again based on the origination rate for that interval. The newly originated taxa were assigned a size equal to their parent's size plus a random size change, Δ_{vol}. Δ_{vol} was drawn from a normal distribution with a mean of zero for the unbiased model and a mean of 0.08 $\log_{10}$ mm^3 for the size-biased model. The average size change for each origination event in the size-biased model was chosen so that the modeled mean size approximated the observed trend in overall mean size across genera. Both models used a standard deviation for Δ_{vol} of 0.348. This standard deviation is the square root of the slope of the linear regression of size variance vs. time across the Phanerozoic. We use this formulation because the slope of the variance-time line is equal to the step variance in diffusive systems (Fig. S6A). This procedure was repeated for each time interval in all models, and reproduced the diversity history observed in our dataset (Fig S6B). The lower bound in the bounded model, -2.31 $\log_{10}$ mm, was set to the size of *Luvula* (phylum Arthropoda, class Ostracoda), which is the smallest genus in our dataset. The lower bound in this model is reflecting — a taxon whose randomly selected Δ_{vol} puts its size smaller than the boundary is assigned a size equal to the boundary plus the positive difference in size it would have been below the boundary. A reflecting boundary was chosen because it is more likely to contribute to increases in overall mean and maximum sizes. However, reflecting boundaries do not produce trends different than cushioning or sticky boundaries (*115*). At the end of each branching simulation, the resulting tree was divided into the 94 geological time intervals used for other analyses. For each interval, the total number of genera, minimum size, mean size, maximum size, and size variance were calculated. The shaded regions in Figures 2 and S4 identify the middle 90% of modeled values of the appropriate model result for a given stage.

We used a likelihood-based method to compare the fit of the observed size distribution in the Pleistocene epoch to the simulated size distributions in the final time step under each of the three models. To estimate the probability density under each model for the final time step, we applied kernel density estimation to the simulated sizes obtained in the final time step in 1000 runs of each model. These estimates were then used to calculate the likelihood for each model given the observed data, which overwhelmingly favored the size-biased model (Table S2).

Analysis of Within vs. Among Taxa Trends

In order to determine if the observed size increase was due to differential diversification or evolutionary size increase within higher taxa, we calculated the expected mean of all animals if there were no size change within higher taxa. We performed this analysis on phyla, classes, orders, and families. To calculate the expected mean trend with no size changes within phyla, we set the size of each genus equal to the mean size of all genera across the Phanerozoic assigned to its corresponding phylum. We then calculated the mean size of all genera across phyla in each time interval. All resultant temporal dynamics in the mean are due entirely to diversification histories within phyla. For example, an increase in mean size could result from the diversification of a large-bodied phylum (e.g., Mollusca) and/or a decrease in diversity of a small-bodied phylum (e.g., Brachiopoda). This procedure was repeated for classes, orders, and families (Fig. S5).

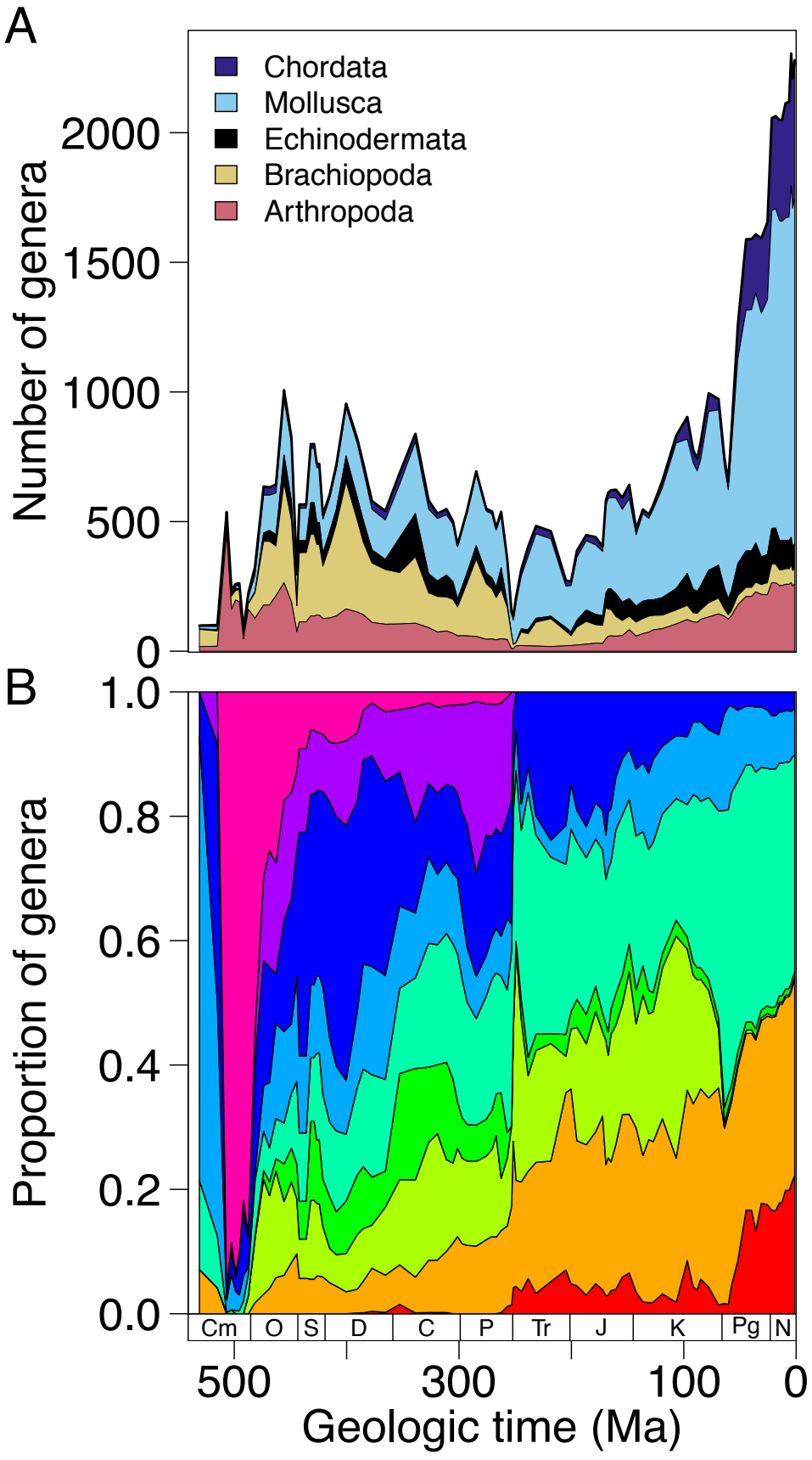
A
Chordata
Mollusca
Echinodermata
Brachiopoda
Arthropoda
Number of genera
2000
1500
1000
500
0
B
Proportion of genera
1.0
0.8
0.6
0.4
0.2
0.0
Cm
O
S
D
C
P
Tr
J
K
Pg
N
500
300
100
0
Geologic time (Ma)

Fig. S1. Taxonomic diversity of Phanerozoic marine animal genera. (A) Total number of genera from the five studied phyla that have stage-resolved stratigraphic ranges and a body size measurement. **(B)** Proportional diversity of the nine Linnaean classes with more than 500 genera. From bottom to top, the classes are: Actinopterygii (red), Bivalvia (orange), Cephalopoda (yellow-green), Crinoidea (green), Gastropoda(blue-green), Ostracoda (light blue), Rhynchonellata (dark blue), Strophomenata (purple), Trilobita (pink). Note that, with the exceptions of decreasing diversity in rhynchonelled brachiopods (top, dark-blue polygon in the post-Paleozoic), the relative diversity remains relatively constant through the Mesozoic. Also note that the last two classes (strophomenid brachiopods and trilobites) became extinct at the end of the Permian. Timescale abbreviations same as in Fig. 1.

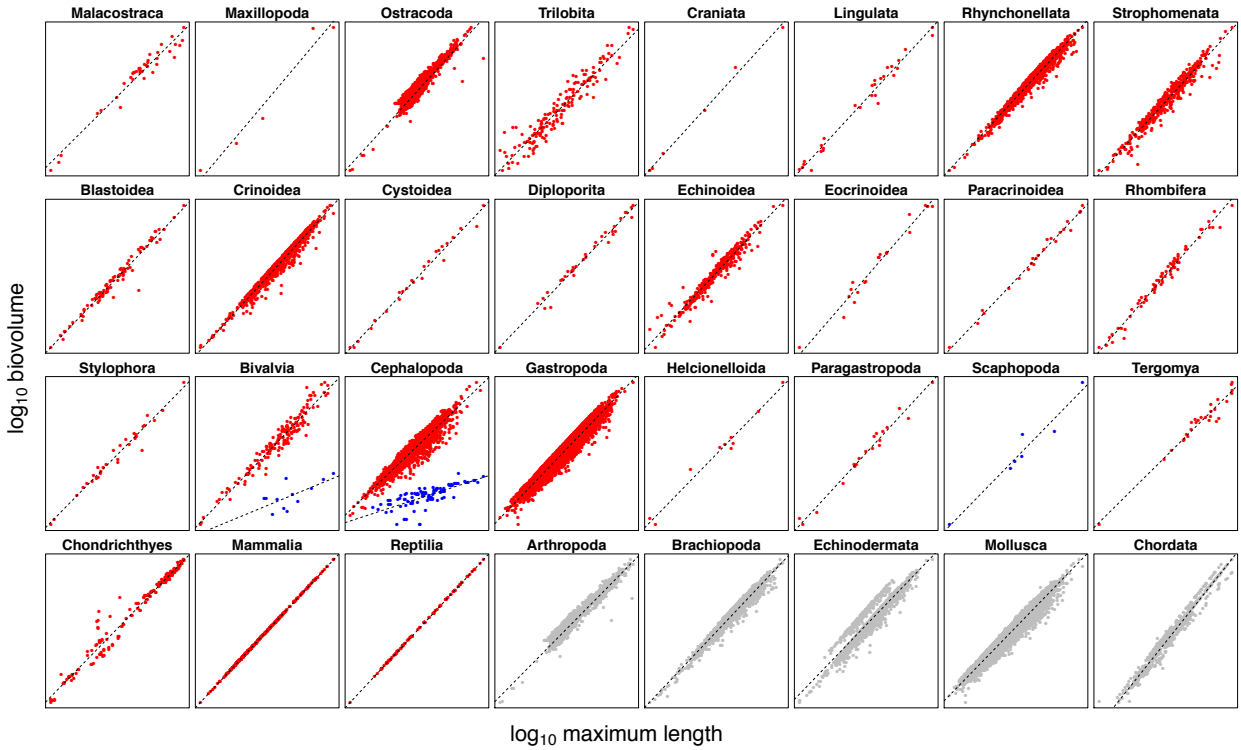

Fig. S2. Linear regressions of maximum linear length vs. biovolume for specimens where biovolume could be estimated from linear measurements. Dashed lines are linear regressions. Classes whose volumes were estimated as an ellipsoid from three linear measurements are plotted in red, and groups whose volume was estimated as a cone are shown in blue. The Mammalia and Reptilia show strong linear relationships because their volumes were estimated from a mass predicted by a log-linear relationship between length and mass in extant taxa (*101,102*). Gray points are for all genera within each phylum. Linear regression equations are given in Table S1.

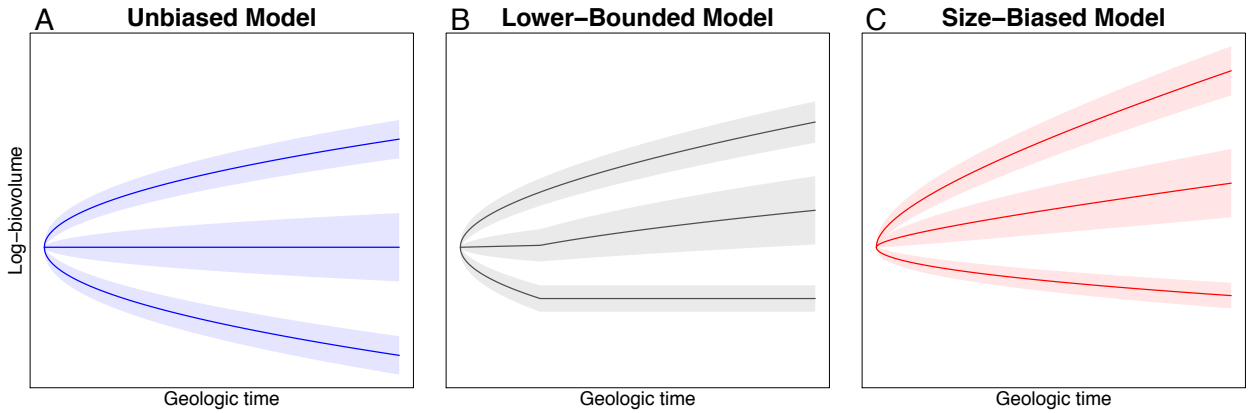

Fig. S3. Three models of evolutionary trends in minimum, mean, and maximum size. Shown are the expected trends (dark lines) and variation among model runs (shaded regions) generated by branching models of size evolution under different sets of constraints. **(A)** The unbiased model assumes descendants are equally likely to be larger or smaller than their ancestors. **(B)** The lower-bounded model assumes descendants are equally likely to be larger or smaller than their ancestors, but there is a minimum to body size. **(C)** The size-biased model assumes descendants are more likely to increase in size relative to their ancestors than they are to decrease in size.

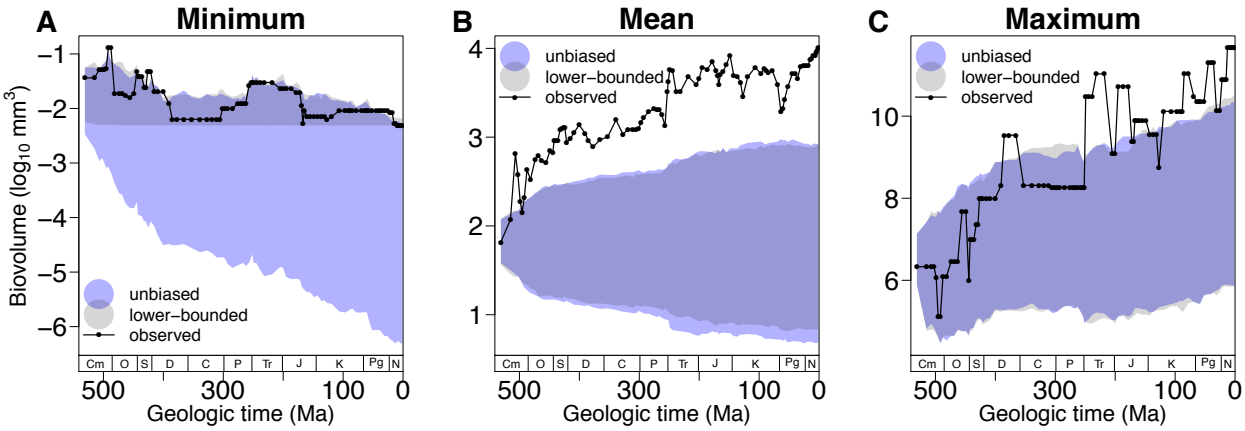

Fig. S4. Comparison of observed biovolume trends to those obtained from stochastic branching models. The colored windows highlight the size space occupied by 90% of the 1,000 model runs. Results for the lower-bounded (gray) and unbiased (blue) are shown to demonstrate these two models produced nearly identical results for the mean and maximum (see Fig. 2 for comparisons of the unbiased and size-biased models). **(A)** minimum, **(B)** mean, and **(C)** maximum sizes. Timescale abbreviations same as in Fig. 1.

Figure S5. Expected mean size if within-taxon size is constant over time. In each panel the size of every genus within each higher taxon is set equal to the mean size of all Phanerozoic genera in that taxon. (**A**) phyla, (**B**) classes, (**C**) orders, and (**D**) families. The expected trend in mean size under constant within-taxon size (red lines) is compared to the observed mean size (black lines). When the two lines plot on top of each other, changes in the observed mean are entirely due to differential diversification among taxa (e.g., families during the Paleozoic). Deviations between the two lines are due to changes in size within higher taxa. When the black line plots below the red line, there are persistent size decreases within taxa (e.g., phyla during the Paleozoic). When the black line plots above the red line, there are persistent size increases within taxa (e.g., classes). Note that in **(B)**, the red line remains relatively flat through the Mesozoic, indicating that the diversification among classes was stagnant.

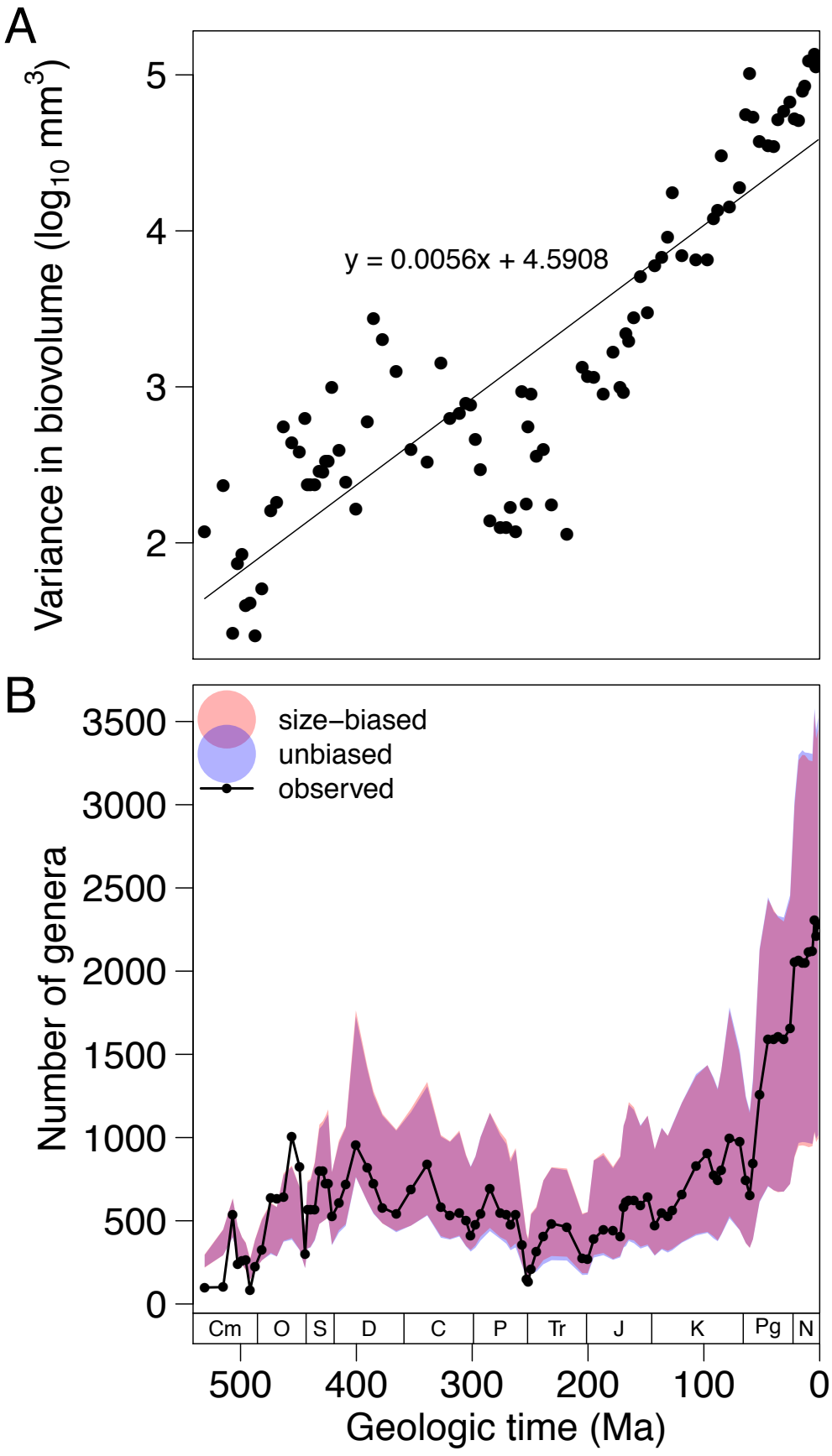
A
Variance in biovolume (log_{10} mm^3)
y = 0.0056x + 4.5908
B
Number of genera
size−biased
unbiased
observed
Cm
O
S
D
C
P
Tr
J
K
Pg
N
Geologic time (Ma)

Fig. S6. Parameterization of evolutionary branching models. (A) Observed relationship between size variance and time. The equation is the corresponding linear regression. The slope of the relationship, which gives the mean change in variance per unit time, was used for the variance in step size in branching models. **(B)** Observed number of genera (black line) compared to the number of genera produced by the middle 90% of model runs. Note that expected diversity is the same for both the size-biased and unbiased models.

taxon	n	intercept	slope	adjusted R^2	cone
Malacostraca	39	-0.7719	2.8411	0.9512	false
Maxillopoda	5	-0.5293	2.945	0.9527	false
Ostracoda	5800	-0.8012	2.7756	0.8788	false
Trilobita	153	-1.055	2.7982	0.9067	false
Craniata	6	-1.6056	3.5648	0.9936	false
Lingulata	28	-0.693	2.8187	0.9783	false
Rhynchonellata	2299	-0.4777	2.8913	0.9685	false
Strophomenata	427	-0.4701	2.8478	0.9454	false
Blastoidea	90	0.5924	2.8471	0.9636	false
Crinoidea	1000	-0.4888	2.9896	0.9621	false
Cystoidea	24	0.5794	2.9317	0.9856	false
Diploporita	34	0.5296	2.9494	0.9812	false
Echinoidea	386	-0.168	2.7457	0.9392	false
Eocrinoidea	19	0.5134	2.8129	0.9664	false
Paracrinoidea	23	0.6022	2.8755	0.9906	false
Rhombifera	69	0.5723	2.9175	0.9773	false
Stylophora	31	0.5531	2.9224	0.9675	false
Bivalvia	161	-0.4833	2.8424	0.9387	false
rudists bivalves	12	-0.2131	1.1271	0.4176	true
Cephalopoda	2923	-0.2839	2.7107	0.9129	false
heteromorphic & uncoiled cephalopods	100	-0.1604	0.9261	0.5349	true
Gastropoda	5846	-0.6987	2.9361	0.9397	false
Helcionelloida	10	-0.883	3.34	0.976	false
Paragastropoda	19	-0.6389	3.0988	0.977	false
Scaphopoda	7	-0.2175	1.5166	0.9386	true
Tergomya	27	-0.457	2.8484	0.951	false
Chondrichthyes	206	-2.6427	3.1522	0.9732	false
Mammalia	385	-1.6174	2.9412	1	false
Reptilia	119	-1.8606	3.088	1	false
Arthropoda	6005	-0.807	2.7352	0.9267	false
Brachiopoda	2765	-0.4865	2.889	0.967	false
Echinodermata	1688	-0.0057	2.7148	0.8726	false
Mollusca	8982	-0.6599	2.916	0.9514	false
Chordata	946	-2.0741	3.0483	0.971	false

Table S1. Linear regressions of biovolume vs. maximum length. Linear regressions of $\log_{10}$ maximum length (mm) vs. $\log_{10}$ biovolume (mm^3) for phyla and classes. Cone column indicates if linear regressions are based on volumes calculated as cones (if not a cone, then calculated as an ellipsoid). The Bivalvia equation does not include rudists, and the Cephalopoda equation does not include uncoiled and heteromorphic forms.

	Size-biased Pleistocene Size Distribution	Unbiased Pleistocene Size Distribution	Bounded Pleistocene Size Distribution
AICc	10218	12220	12203
Akaike weight	> 0.9999	< 0.0001	< 0.0001

Table S2. Results of model comparisons for the Phanerozoic trend in Pleistocene size distributions. Lower AICc and higher Akaike weights indicate more support for a given model. The size-biased model is strongly supported.

	logL	AICc	K	Akaike Weight	Akaike Weight Single-Phase Model Comparison
Random Walk	57.2	-110.2	2	0.001	0.294
Driven Trend	59.1	-111.9	3	0.001	0.706
Stasis	-60.3	124.7	2	0.000	0.000
Two-Phase (Driven Trend/Random Walk)	64.0	-117.3	5	0.020	n/a
Three-Phase (Driven Trend/Stasis/Driven Trend)	71.4	-125.1	8	0.978	n/a

Table S3. Results of model comparison for the entire Phanerozoic with the marine mammals and reptiles removed. Lower AICc and higher Akaike weights indicate more support for a given model. logL is the log likelihood; K is the number of free parameters in each model; Three-Model Comparison Akaike Weight compares only the three single-phase models. The two-phase model has a breakpoint at the Permian/Triassic boundary. The three-phase model has breakpoints at the Permian/Triassic and Cretaceous/Paleogene boundaries. The best-fit model for each phase is used in multiphase models. With tetrapods removed, the three-phase model still has the most support.

Supplementary Data File. Sizes and stratigraphic ranges

PaleoDB_taxon_no: taxon number for the Paleobiology Database

taxon_name: genus name

phylum: Linnaean phylum

class: Linnaean class

fad_int: interval of first appearance in the fossil record

fad_age: age of the base of fad_int

lad_int: interval of last appearance in the fossil record

lad_age: age of the top of lad_int

size_ref: source of size, corresponds to reference number

range_ref: source of stratigraphic range, corresponds to reference number

log10_volume: $\log_{10}$ transformed biovolume (mm^3)

log10_max_length: $\log_{10}$ transformed maximum dimension (mm)

REFERENCES

1. R. H. Peters, *The Ecological Implications of Body Size* (Cambridge Univ. Press, Cambridge, 1983).

2. J. H. Brown, *Macroecology* (Univ. of Chicago Press, Chicago, 1995).

3. E. D. Cope, On the evolution of the Vertebrata, progressive and retrogressive (Continued). *Am. Nat.* **19**, 234–247 (1885). doi:10.1086/273900

4. E. D. Cope, *The Primary Factors of Organic Evolution* (Open Court, London, 1896).

5. C. J. J. Depéret, *The Transformations of the Animal World* (Paul, Trench, Trübner; London, 1909).

6. N. D. Newell, Phyletic size increase, an important trend illustrated by fossil invertebrates. *Evolution* **3**, 103–124 (1949). Medline doi:10.2307/2405545

7. R. K. Bambach, Seafood through time: Changes in biomass, energetics, and productivity in the marine ecosystem. *Paleobiology* **19**, 372–397 (1993).

8. J. G. Kingsolver, D. W. Pfennig, Individual-level selection as a cause of Cope's rule of phyletic size increase. *Evolution* **58**, 1608–1612 (2004). Medline doi:10.1111/j.0014-3820.2004.tb01740.x

9. B. Rensch, Histological changes correlated with evolutionary changes of body size. *Evolution* **2**, 218–230 (1948). Medline doi:10.2307/2405381

10. J. Alroy, Cope's rule and the dynamics of body mass evolution in North American fossil mammals. *Science* **280**, 731–734 (1998). Medline doi:10.1126/science.280.5364.731

11. A. J. Arnold, D. C. Kelly, W. C. Parker, Causality and Cope's Rule: Evidence from the planktonic foraminifera. *J. Paleontol.* **69**, 203–210 (1995).

12. B. A. Maurer, The evolution of body size in birds. I. Evidence for non-random diversification. *Evol. Ecol.* **12**, 925–934 (1998). doi:10.1023/A:1006512121434

13. M. Laurin, The evolution of body size, Cope's rule and the origin of amniotes. *Syst. Biol.* **53**, 594–622 (2004). Medline doi:10.1080/10635150490445706

14. D. W. E. Hone, T. M. Keesey, D. Pisani, A. Purvis, Macroevolutionary trends in the Dinosauria: Cope's rule. *J. Evol. Biol.* **18**, 587–595 (2005). Medline doi:10.1111/j.1420-9101.2004.00870.x

15. P. M. Novack-Gottshall, M. A. Lanier, Scale-dependence of Cope's rule in body size evolution of Paleozoic brachiopods. *Proc. Natl. Acad. Sci. U.S.A.* **105**, 5430–5434 (2008). Medline doi:10.1073/pnas.0709645105

16. D. Jablonski, Body-size evolution in Cretaceous molluscs and the status of Cope's Rule. *Nature* **385**, 250–252 (1997). doi:10.1038/385250a0

17. S. J. Gould, Trends as changes in variance: A new slant on progress and directionality in evolution. *J. Paleontol.* **62**, 319–329 (1988).

18. D. S. Moen, Cope's rule in cryptodiran turtles: Do the body sizes of extant species reflect a trend of phyletic size increase? *J. Evol. Biol.* **19**, 1210–1221 (2006). Medline doi:10.1111/j.1420-9101.2006.01082.x

19. M. J. Monroe, F. Bokma, Little evidence for Cope's rule from Bayesian phylogenetic analysis of extant mammals. *J. Evol. Biol.* **23**, 2017–2021 (2010). Medline doi:10.1111/j.1420-9101.2010.02051.x

20. R. J. Butler, A. Goswami, Body size evolution in Mesozoic birds: Little evidence for Cope's rule. *J. Evol. Biol.* **21**, 1673–1682 (2008). Medline doi:10.1111/j.1420-9101.2008.01594.x

21. J. H. Knouft, L. M. Page, The evolution of body size in extant groups of North American freshwater fishes: Speciation, size distributions, and Cope's rule. *Am. Nat.* **161**, 413–421 (2003). Medline doi:10.1086/346133

22. S. M. Stanley, An explanation for Cope's Rule. *Evolution* **27**, 1–26 (1973). doi:10.2307/2407115

23. Materials and methods are available as supplementary materials on *Science* Online.

24. J. J. Sepkoski Jr., A compendium of fossil marine genera. *Bull. Am. Paleontol.* **363**, 1–500 (2002).

25. S. J. Gould, E. S. Vrba, Exaptation-a missing term in the science of form. *Paleobiology* **8**, 4–15 (1982).

26. D. Pauly, *Gasping Fish and Panting Squids: Oxygen, Temperature and the Growth of Water-Breathing Animals* (International Ecology Institute, Oldendorf, Germany, 2010).

27. T. W. Dahl, E. U. Hammarlund, A. D. Anbar, D. P. Bond, B. C. Gill, G. W. Gordon, A. H. Knoll, A. T. Nielsen, N. H. Schovsbo, D. E. Canfield, Devonian rise in atmospheric oxygen correlated to the radiations of terrestrial plants and large predatory fish. *Proc. Natl. Acad. Sci. U.S.A.* **107**, 17911–17915 (2010). Medline doi:10.1073/pnas.1011287107

28. E. A. Sperling, C. A. Frieder, A. V. Raman, P. R. Girguis, L. A. Levin, A. H. Knoll, Oxygen, ecology, and the Cambrian radiation of animals. *Proc. Natl. Acad. Sci. U.S.A.* **110**, 13446–13451 (2013). Medline doi:10.1073/pnas.1312778110

29. G. J. Vermeij, The evolutionary interaction among species: Selection, escalation, and coevolution. *Annu. Rev. Ecol. Syst.* **25**, 219–236 (1994). doi:10.1146/annurev.es.25.110194.001251

30. H. D. Holland, The oxygenation of the atmosphere and oceans. *Philos. Trans. R. Soc. London Ser. B* **361**, 903–915 (2006). Medline doi:10.1098/rstb.2006.1838

31. S. Finnegan, C. R. McClain, M. A. Kosnik, J. L. Payne, Escargots through time: An energetic comparison of marine gastropod assemblages before and after the Mesozoic Marine Revolution. *Paleobiology* **37**, 252–269 (2011). doi:10.1666/09066.1

32. J. Alroy, M. Aberhan, D. J. Bottjer, M. Foote, F. T. Fürsich, P. J. Harries, A. J. Hendy, S. M. Holland, L. C. Ivany, W. Kiessling, M. A. Kosnik, C. R. Marshall, A. J. McGowan, A. I. Miller, T. D. Olszewski, M. E. Patzkowsky, S. E. Peters, L. Villier, P. J. Wagner, N. Bonuso, P. S. Borkow, B. Brenneis, M. E. Clapham, L. M. Fall, C. A. Ferguson, V. L.

Hanson, A. Z. Krug, K. M. Layou, E. H. Leckey, S. Nürnberg, C. M. Powers, J. A. Sessa, C. Simpson, A. Tomasovych, C. C. Visaggi, Phanerozoic trends in the global diversity of marine invertebrates. *Science* **321**, 97–100 (2008). Medline doi:10.1126/science.1156963

33. A. I. Miller, M. Aberhan, D. P. Buick, K. V. Bulinski, C. A. Ferguson, A. J. W. Hendy, W. Kiessling, Phanerozoic trends in the global geographic disparity of marine biotas. *Paleobiology* **35**, 612–630 (2009). doi:10.1666/0094-8373-35.4.612

34. R. A. Krause, J. A. Stempien, M. J. Kowalewski, A. I. Miller, Body size estimates from the literature: Utility and potential for macroevolutionary studies. *Palaios* **22**, 60–73 (2007). doi:10.2110/palo.2005.p05-122r

35. M. A. Kosnik, D. Jablonski, R. Lockwood, P. M. Novack-Gottshall, Quantifying molluscan body size in evolutionary and ecological analyses: Maximizing the return on data-collection efforts. *Palaios* **21**, 588–597 (2006). doi:10.2110/palo.2006.p06-012r

36. A. Williams *et al*., *Treatise on Invertebrate Paleontology. Part H, Brachiopoda (Revised), vols. 1-6* (Geological Society of America and Paleontological Institute; Boulder, CO, and Lawrence, KS, 2007).

37. J. B. Knight *et al*., *Treatise on Invertebrate Paleontology. Part I, Mollusca 1: Mollusca General Features, Scaphopoda, Amphineura, Monoplacophora, Gastropoda. General Features, Archaeogastropoda and some (mainly Paleozoic) Caenogastropoda and Opisthobranchia* (Geological Society of America and University of Kansas Press; Boulder, CO, and Lawrence, KS, 1960).

38. C. Teichert *et al*., *Treatise on Invertebrate Paleontology. Part K, Mollusca 3: Cephalopoda. General Features, Endoceratoidea, Actinoceratoidea, Nautiloidea, Bactritoidea* (Geological Society of America and University of Kansas Press; Boulder, CO, and Lawrence, KS, 1964).

39. W. J. Arkell *et al*., *Treatise on Invertebrate Paleontology. Part L, Mollusca 4: Cephalopoda, Ammonoidea* (Geological Society of America and University of Kansas Press; Boulder, CO, and Lawrence, KS, 1957).

40. W. M. Furnish, B. F. Glenister, J. Küllman, Z. Zuren, *Treatise on Invertebrate Paleontology. Part L, Mollusca 4 (Revised), vol. 2: Carboniferous and Permian Ammonoidea (Goniatitida and Prolecanitida)* (Geological Society of America and University of Kansas Press; Boulder, CO, and Lawrence, KS, 2009).

41. C. W. Wright, J. H. Calloman, M. K. Howarth, *Treatise on Invertebrate Paleontology. Part L, Mollusca 4 (Revised), vol. 4: Cretaceous Ammonoidea* (Geological Society of America and University of Kansas Press; Boulder, CO, and Lawrence, KS, 1996).

42. L. R. Cox *et al*., *Treatise on Invertebrate Paleontology. Part N, Mollusca 6, Bivalvia, vol 1 and 2* (Geological Society of America and University of Kansas Press; Boulder, CO, and Lawrence, KS, 1969).

43. L. R. Cox *et al*., *Treatise on Invertebrate Paleontology. Part N, Mollusca 6, Bivalvia, vol 3* (Geological Society of America and University of Kansas Press; Boulder, CO, and Lawrence, KS, 1971).

44. H. J. Harrington *et al*., *Treatise on Invertebrate Paleontology. Part O, Arthropoda 1: General Features, Protarthropoda, Euarthropoda General Features, Trilobitomorpha* (Geological Society of America and University of Kansas Press; Boulder, CO, and Lawrence, KS, 1959).

45. H. B. Whittington *et al*., *Treatise on Invertebrate Paleontology. Part O, Arthropoda 1, Trilobita (Revised), vol. 1: Introduction, Order Agnostida, Order Redlichiida* (Geological Society of America and University of Kansas Press; Boulder, CO, and Lawrence, KS, 1997).

46. L. Størmer, A. Petrunkevitch, J. W. Hedgpeth, *Treatise on Invertebrate Paleontology. Part P, Arthropoda 2: Chelicerata with sections on Pycnogonida and Palaeoisopus* (Geol. Soc. Am. & Univ. Kansas Press, Boulder, CO & Lawrence, KS, 1956).

47. R. H. Benson *et al*., *Treatise on Invertebrate Paleontology. Part Q, Arthropoda 3: Crustacea, Ostracoda* (Geological Society of America and University of Kansas Press; Boulder, CO, and Lawrence, KS, 1961).

48. H. K. Brooks *et al*., *Treatise on Invertebrate Paleontology. Part R, Arthropoda 4, vol 1 and 2: Crustacea (Exclusive of Ostracoda), Myriapoda, Hexapoda* (Geological Society of America and University of Kansas Press; Boulder, CO, and Lawrence, KS, 1969).

49. F. M. Carpenter, *Treatise on Invertebrate Paleontology. Part R, Arthropoda 4, vol 3 and 4: Hexapoda* (Geological Society of America and University of Kansas Press; Boulder, CO, and Lawrence, KS, 1992).

50. H. H. Beaver *et al*., *Treatise on Invertebrate Paleontology. Part S, Echinodermata 1: Echinodermata General Features, Homalozoa, Crinozoa, exclusive of Crinoidea, vol. 1* (Geological Society of America and University of Kansas Press; Boulder, CO, and Lawrence, KS, 1967).

51. G. Ubaghs *et al*., *Treatise on Invertebrate Paleontology. Part T, Echinodermata 2: Crinoidea* (Geological Society of America and University of Kansas Press; Boulder, CO, and Lawrence, KS, 1978).

52. H. Hess, C. G. Messing, W. I. Ausich, *Treatise on Invertebrate Paleontology. Part T, Echinodermata 2 (Revised): Crinoidea* (Paleontological Institute, Lawrence, KS, 2011).

53. J. W. Durham *et al*., *Treatise on Invertebrate Paleontology. Part U, Echinodermata 3: Asterozoa—Echinozoa* (Geological Society of America and University of Kansas Press; Boulder, CO, and Lawrence, KS, 1966).

54. D. A. Clark *et al*., *Treatise on Invertebrate Paleontology. Part W, Miscellanea: Supplement 2: Conodonta* (Geological Society of America and University of Kansas Press; Boulder, CO, and Lawrence, KS, 1981).

55. W. Wenz, in *Handbuch der Palaozoologie (Handbook of Paleozoology)*, O. H. Schindewolf, Ed. (Gebruder Borntraeger, Berlin, 1938).

56. B. F. Ellis, A. R. Messina, *Catalogue of Ostracoda* (American Museum of Natural History, New York, 1954–1994).

57. M. Huber, *Compendium of Bivalves. A Full-color Guide to 3,300 of the World's Marine Bivalves. A Status on Bivalvia after 250 Years of Research* (ConchBooks, Hackenheim, Germany, 2010).

58. K. A. Frickhinger, *Fossil Atlas, Fishes* (Mergus, Blacksburg, VA, 1995).

59. Y. A. Orlov, Ed., *Fundamentals of Paleontology, Vol. XI: Agnatha, Pisces (Osnovy Paleontologii; translated from Russian)* (Israel Program for Scientific Translations, Jerusalem, 1967).

60. D. K. Sarko, D. P. Domning, L. Marino, R. L. Reep, Estimating body size of fossil sirenians. *Mar. Mamm. Sci.* **26**, 937–959 (2010). doi:10.1111/j.1748-7692.2010.00384.x

61. I. S. Zalmout, P. D. Gingerich, Late Eocene sea cows (Mammalia, Sirenia) from Wadi Al Hitan in the Fayum Basin, Egypt. *Univ. Mich. Pap. Paleontol.* **37**, 1–158 (2012).

62. O. Kuhn, *Handbuch der Paläoherpetologie (Encyclopedia of Paleoherpetology)* (Pfeil, Stuttgart, Germany, 2000).

63. M. L. D. Palomares, D. Pauly, *SeaLifeBase* (2013), http://www.sealifebase.org/.

64. R. L. Carroll, *Patterns and Processes of Vertebrate Evolution* (Cambridge Univ. Press, New York, 1997).

65. R. L. Carroll, *Vertebrate Paleontology and Evolution* (Freeman, New York, 1988).

66. J. Chaline, *Paleontology of Vertebrates* (Springer-Verlag, New York, 1990).

67. M. J. Benton, *Vertebrate Palaeontology* (Blackwell, Malden, MA, 2005).

68. H. A. Nicholson, R. Lydekker, *A Manual of Palaeontology* (Blackwood, Edinburgh, UK, 1889).

69. D. Dixon, *The Complete Book of Dinosaurs* (Hermes House, Leicester, UK, 2006).

70. D. J. Bottjer, W. Etter, J. W. Hagadorn, Eds., *Exceptional Fossil Preservation: A Unique View on the Evolution of Marine Life* (Columbia Univ. Press, New York, 2001).

71. P. L. Lutz, J. A. Musick, *The Biology of Sea Turtles* (CRC Press, Boca Raton, FL, 1996).

72. J. M. Calloway, E. L. Nicholls, *Ancient Marine Reptiles* (Academic Press, London, 1997).

73. D. Palmer, *The Illustrated Encyclopedia of Dinosaurs and Prehistoric Creatures* (Chartwell, New York, 2011).

74. D. S. Farner, J. R. King, K. C. Parkes, *Avian Biology, Voume VIII* (Academic Press, New York, 1985).

75. D. K. Publishing, *Prehistoric Life: The Definitive Visual History of Life on Earth* (DK Publishing, London, American ed. 1, 2009).

76. R. Ellis, *Sea Dragons: Predators of the Prehistoric Oceans* (Univ. of Kansas Press, Lawrence, KS, 2003).

77. B. F. Kosch, A revision of the skeletal reconstruction of *Shonisaurus popularis* (Reptilia: Ichthyosauria). *J. Vertebr. Paleontol.* **10**, 512–514 (1990). doi:10.1080/02724634.1990.10011833

78. W. Auffenberg, *Anomalofhis bolcensis* (Massalongo), a new genus of fossil snake from the Italian Eocene. *BREVIORA Mus. Comp. Zool.* **114**, 1–16 (1959).

79. E. Buffetaut, C. Colleté, B. Dubus, J.-L. Petit, The 'sauropod' from the Albian of Mesnil-Saint-Père (Aube, France): A pliosaur, not a dinosaur. *Assoc. Géol. Auboise Bull. Ann. Sainte-Savine* **26**, 3–8 (2005).

80. C. L. Camp, California mosasaurs. *Mem. Univ. Calif.* **13**, 1–68 (1942).

81. J. P. Davidson, M. J. Everhart, Fictionalized facts: 'The Young Fossil Hunters' by Charles H. Sternberg. *Trans. Kans. Acad. Sci.* **117**, 41–54 (2014). 10.1660/062.117.0106 doi:10.1660/062.117.0106

82. M. W. Maisch, A. T. Matzke, The Ichthyosauria. *Stuttgarter Beiträge Naturkunde Ser. B (Geol. Paläontol.)* **298**, 1–159 (2000).

83. S. P. Welles, Elasmosaurid plesiosaurs with description of new material from California and Colorado. *Mem. Univ. Calif.* **13**, 125–254 (1943).

84. R. Motani, N. Minoura, T. Ando, Ichthyosaurian relationships illuminated by new primitive skeletons from Japan. *Nature* **393**, 255–257 (1998). 10.1038/30473 doi:10.1038/30473

85. L. F. Noè, J. Liston, M. Evans, The first relatively complete exoccipital-opisthotic from the braincase of the Callovian pliosaur. *Liopleurodon. Geol. Mag.* **140**, 479–486 (2003). 10.1017/S0016756803007829 doi:10.1017/S0016756803007829

86. J.-C. Rage, *Palaeophis colossaeus* nov. sp. (le plus grand Serpent connu?) de l'Eocène du Mali et le problème du genre chez les Palaeopheinae. *C. R.Acad. Sci. Paris* **3**, 1741–1744 (1983).

87. K. Shimada, M. V. Fernandes, *Ichthyornis* sp. (Aves: Ichthyornithiformes) from the lower Turonian (Upper Cretaceous) of western Kansas. *Trans. Kans. Acad. Sci.* **109**, 21–26 (2006). doi:10.1660/0022-8443(2006)109[21:ISAIFT]2.0.CO;2

88. J. A. Massare, Swimming capabilities of mesozoic marine reptiles: Implications for method of predation. *Paleobiology* **14**, 187–205 (1988).

89. M. T. Young, S. L. Brusatte, M. B. de Andrade, J. B. Desojo, B. L. Beatty, L. Steel, M. S. Fernández, M. Sakamoto, J. I. Ruiz-Omeñaca, R. R. Schoch, The cranial osteology and feeding ecology of the metriorhynchid crocodylomorph genera *Dakosaurus* and *Plesiosuchus* from the late Jurassic of Europe. *PLOS ONE* **7**, e44985 (2012). 10.1371/journal.pone.0044985 Medline doi:10.1371/journal.pone.0044985

90. F. R. O'Keefe, L. M. Chiappe, Viviparity and K-selected life history in a Mesozoic marine plesiosaur (Reptilia, *Sauropterygia*). *Science* **333**, 870–873 (2011). 10.1126/science.1205689 Medline doi:10.1126/science.1205689

91. M. J. Everhart, *Oceans of Kansas Paleontology* (2014), http://oceansofkansas.com.

92. University of Michigan, *Animal Diversity Web* (2014), http://animaldiversity.ummz.umich.edu.

93. M. A. Kazlev, R. Santos, R. Perkins, Eds., *Palaeos: Life Through Deep Time* (2014), http://palaeos.com.

94. Yale Peabody Museum, *Yale Peabody Museum* (2014), http://peabody.yale.edu.

95. BBC, *Prehistoric Life: Sea Monsters* (2014), http://www.bbc.co.uk/sn/prehistoric_life/tv_radio/wwseamonsters/.

96. D. Peters, Ed., *Reptile Evolution* (2014), http://www.reptileevolution.com.

97. P. Files, *Paleo Files* (2014), https://sites.google.com/site/paleofilescom/.

98. M. A. Etnier, C. W. Fowler, Comparison of size selectivity between marine mammals and commercial fisheries with recommendations for restructuring management policies. *NOAA Tech. Memo. NMFS-AFSC* **159**, 1–274 (2005).

99. A. Clauset, How large should whales be? *PLOS ONE* **8**, e53967 (2013). Medline doi:10.1371/journal.pone.0053967

100. R. Froese, D. Pauly, *FishBase* (2013), http://www.fishbase.org/.

101. M. Silva, Allometric scaling of body length: Elastic or geometric similarity in mammalian design. *J. Mammal.* **79**, 20–32 (1998). doi:10.2307/1382839

102. S. Meiri, Length–weight allometries in lizards. *J. Zool.* **281**, 218–226 (2010).

103. P. J. O. Miller, M. P. Johnson, P. L. Tyack, E. A. Terray, Swimming gaits, passive drag and buoyancy of diving sperm whales *Physeter macrocephalus*. *J. Exp. Biol.* **207**, 1953–1967 (2004). Medline doi:10.1242/jeb.00993

104. F. R. H. Jones, N. B. Marshall, The structure and functions of the the teleostean swimbladder. *Biol. Rev. Camb. Philos. Soc.* **28**, 16–82 (1953). doi:10.1111/j.1469-185X.1953.tb01370.x

105. H. D. Baldridge Jr., Sinking factors and average densities of Florida sharks as functions of liver buoyancy. *Copeia* **1970**, 744–754 (1970). doi:10.2307/1442317

106. J.-L. Dommergues, S. Montuire, P. Neige, Size patterns through time: The case of the Early Jurassic ammonite radiation. *Paleobiology* **28**, 423–434 (2002). doi:10.1666/0094-8373(2002)028<0423:SPTTTC>2.0.CO;2

107. J. L. Payne, Evolutionary dynamics of gastropod size across the end-Permian extinction and through the Triassic recovery interval. *Paleobiology* **31**, 269–290 (2005). doi:10.1666/0094-8373(2005)031[0269:EDOGSA]2.0.CO;2

108. H. Cummins, E. N. Powell, R. J. Stanton Jr., G. M. Staff, The size-frequency distribution in palaeoecology: Effects of taphonomic processes during formation of molluscan death assemblages in Texas bays. *Palaeontology* **29**, 495–518 (1986).

109. A. J. W. Hendy, The influence of lithification on Cenozoic marine biodiversity trends. *Paleobiology* **35**, 51–62 (2009). doi:10.1666/07047.1

110. J. A. Sessa, M. E. Patzkowsky, T. J. Bralower, The impact of lithification on the diversity, size distribution, and recovery dynamics of marine invertebrate assemblages. *Geology* **37**, 115–118 (2009). doi:10.1130/G25286A.1

111. J. Hagadorn, R. Dott, D. Damrow, Stranded on a Late Cambrian shoreline: Medusae from central Wisconsin. *Geology* **30**, 147–150 (2002). doi:10.1130/0091-7613(2002)030<0147:SOALCS>2.0.CO;2

112. G. Hunt, *paleoTS: Analyze paleontological time-series* (2012), http://CRAN.R-project.org/package=paleoTS.

113. G. Hunt, Fitting and comparing models of phyletic evolution: Random walks and beyond. *Paleobiology* **32**, 578–601 (2006). doi:10.1666/05070.1

114. G. Hunt, in *From Evolution to Geobiology: Research Questions Driving Paleontology at the Start of a New Century*, P. H. Kelley, R. K. Bambach, Eds. (Paleontological Society, Lawrence, KS, 2008), pp. 117–131.

115. D. W. McShea, Mechanisms of large-scale evolutionary trends. *Evolution* **48**, 1747–1763 (1994). doi:10.2307/2410505

116. D. M. Raup, S. J. Gould, T. J. M. Schopf, D. S. Simberloff, Stochastic models of phylogeny and the evolution of diversity. *J. Geol.* **81**, 525–542 (1973). doi:10.1086/627905

117. M. Foote, Origination and extinction components of taxonomic diversity: General problems. *Paleobiology* **26** (suppl. 4), 74–102 (2000). doi:10.1666/0094-8373(2000)26[74:OAECOT]2.0.CO;2

118. A. Hassanin, F. Delsuc, A. Ropiquet, C. Hammer, B. Jansen van Vuuren, C. Matthee, M. Ruiz-Garcia, F. Catzeflis, V. Areskoug, T. T. Nguyen, A. Couloux, Pattern and timing of diversification of Cetartiodactyla (Mammalia, Laurasiatheria), as revealed by a comprehensive analysis of mitochondrial genomes. *C. R. Biol.* **335**, 32–50 (2012). Medline doi:10.1016/j.crvi.2011.11.002

119. J. E. Randall, Size of the great white shark (*Carcharodon*). *Science* **181**, 169–170 (1973). Medline doi:10.1126/science.181.4095.169

120. S. C. Morris, J. S. Peel, Articulated halkieriids from the Lower Cambrian of North Greenland and their role in early protostome evolution. *Philos. Trans. R. Soc. London Ser. B* **347**, 305–358 (1995). doi:10.1098/rstb.1995.0029